Soft Matter

PAPER

View Article Online
View Journal | View Issue

Cite this: *Soft Matter*, 2015, 11, 8975

Bimodality and re-entrant behaviour in the hierarchical self-assembly of polymeric nanoparticles†

Sarika C. K.,[a] Gaurav Tomar,[b] J. K. Basu*[c] and Uwe Thiele[de]

Received 22nd August 2015,
Accepted 17th September 2015

DOI: 10.1039/c5sm02108a

www.rsc.org/softmatter

We show that a film of a suspension of polymer grafted nanoparticles on a liquid substrate can be employed to create two-dimensional nanostructures with a remarkable variation in the pattern length scales. The presented experiments also reveal the emergence of concentration-dependent bimodal patterns as well as re-entrant behaviour that involves length scales due to dewetting and compositional instabilities. The experimental observations are explained through a gradient dynamics model consisting of coupled evolution equations for the height of the suspension film and the concentration of polymer. Using a Flory–Huggins free energy functional for the polymer solution, we show in a linear stability analysis that the thin film undergoes dewetting and/or compositional instabilities depending on the concentration of the polymer in the solution. We argue that the formation *via* 'hierarchical self-assembly' of various functional nanostructures observed in different systems can be explained as resulting from such an interplay of instabilities.

1 Introduction

Nature abounds in sophisticated functional materials created through self-assembly of nanoscale structures.[1,2] In part, this has motivated much effort in understanding the mechanisms that control self-assembly and self-organisation at multiple length scales.[3–5] On the other hand, precise control of such hierarchical self-organisation would offer elegant and efficient bottom-up strategies to create artificial, complex multifunctional materials with varied optical, electronic or magnetic properties.[6,7] Drying-mediated assembly of nanoparticles has been shown to allow for the formation of well-ordered large-scale two-dimensional (2D) arrays.[8–10] Diverse 2D patterns of nanoparticles can be generated also by dewetting of nanoparticle laden thin films.[10–13] However, a complete theoretical understanding of the phenomenon, and thus its control, is lacking primarily due to the complexity that results from the combination of dewetting, decomposition, evaporation and adsorption processes. In this study we report the formation of hierarchical 2D assemblies of clusters of metal nanoparticles grafted with polymers created at the air–water interface. Experiments for a range of concentrations reveal qualitatively different patterns in the deposited thin film of nanoparticle suspensions including the emergence of unique bimodal spatial patterns with widely separated lateral length scales, within a range of intermediate concentrations. In the process we also observe the appearance of an interesting re-entrant behaviour of pattern formation above some critical concentrations. We obtained similar transitions in the pattern length scale with increasing concentration for un-grafted PS solutions. Performing a linear stability analysis (LSA) of coupled evolution equations for solute concentration and height of the thin film, we show that a small length scale compositional instability within the film can interact with a large length scale dewetting instability of the film. The interplay is predicted to result in the formation of a laterally patterned film with a bimodal length scale distribution. The model predicts the experimentally observed transition from unimodal to bimodal structuring, the corresponding disparate lateral length scales and the re-entrant behaviour. Overall, it provides a framework to obtain morphological phase diagrams for the spontaneous creation of hierarchical arrangements of soft polymer based nanostructures at an interface through self-assembly and self-organisation processes.

2 Materials and methods

The experiments reported here are performed using thiolated-polystyrene (PST) grafted spherical gold nanoparticles (PGNP) synthesized by the grafting-to method (see the ESI† for details

[a] *Department of Physics, Indian Institute of Science, Bangalore, India*
[b] *Department of Mechanical Engineering, Indian Institute of Science, Bangalore, India. E-mail: gtom@mecheng.iisc.ernet.in*
[c] *Department of Physics, Indian Institute of Science, Bangalore, India. E-mail: basu@physics.iisc.ernet.in*
[d] *Institut für Theoretische Physik, Westfälische Wilhelms-Universität Münster, Wilhelm Klemm Str. 9, D-48149 Münster, Germany*
[e] *Center of Nonlinear Science (CeNoS), Westfälische Wilhelms Universität Münster, Corrensstr. 2, 48149 Münster, Germany. E-mail: u.thiele@uni-muenster.de*

† Electronic supplementary information (ESI) available. See DOI: 10.1039/c5sm02108a

Table 1 Characteristics of the PGNPs used for the preparation of thin films

Sample index	M_w (g mol^{-1})	d_c (nm)	σ (nm^{-2})	d_{melt} (nm)	R_h (nm)
PGNP53K	53 000	3.1	1	17	27
PGNP3K	3000	3.1	1.33	7.4	8

of synthesis and characterization). Detailed specification of the relevant parameters of the PGNPs used in this work is provided in Table 1.‡ The reported results are primarily based on PST3K and PGNP3K samples with supporting data for PGNP53K as well. To prepare thin suspension films, we first formed a suspension of different concentrations of PGNPs in chloroform, typically ~0.1–2 mg ml^{-1}. A total volume of 30 μl of the respective solutions is uniformly spread onto an air–water interface in a Langmuir–Blodgett (LB) trough (KSV NIMA) of area 140 cm^2 using a Hamilton syringe in steps of 2 μl transferred at an interval of a few minutes at different locations of the LB trough. The total volume of solution to be transferred was chosen so as to obtain a reasonable density of PGNPs on the surface. Since chloroform has an extremely high spreading coefficient on water, the transferred PGNP solution spreads across the surface of the LB trough to form a uniform film of chloroform suspension of respective PGNPs. Evaporation of chloroform leaves a PGNP layer at the air–water interface which is compressed by moving the LB barrier with a speed of 5 mm min^{-1} and surface pressure is measured using a Wilhelmy plate. At a surface pressure of 5 mN m^{-1}, the compression is stopped and the film is transferred to the appropriately cleaned glass substrate by withdrawing the substrate, vertically, from the water subphase through the PGNP layer with a speed of 0.5 mm min^{-1}, to avoid distortion of this layer morphology formed on water. The temperature of the LB water subphase was maintained at 25 °C during the entire process. After evaporation of water in the transferred PGNP films, they were imaged by atomic force microscopy (AFM, NT MDT) operating in the tapping mode to ensure minimal distortion of the morphology.

3 Results and discussion

3.1 Experimental results

Fig. 1a–d show a series of AFM images of the transferred PGNP films for different spreading concentrations of PGNP3K solutions. For very low concentrations (~0.05 mg ml^{-1}), the lateral pattern length scale is ~800 nm–1 μm as seen in Fig. 1a. With increasing concentration we observe a transition in the morphology that becomes dominated by an emerging smaller lateral length scale (~30–60 nm) related to the size and distance of spheroidal clusters of particles (Fig. 1b and c). The large scale perforated arrangement of the clusters is governed by a much larger length scale (also *cf.* Fig. S9 of the ESI†). The corresponding pair correlation function, $g(r)$, shows a pronounced peak at a distance $r \sim 50$ nm, *i.e.* at the length scale of cluster size and spacing. The height of these structures is similar to the diameter of individual PGNPs (~7–9 nm) within the clusters, clearly indicating the formation of PGNP monolayers. For larger concentrations (1.6 mg ml^{-1}), we observe an interesting re-entrant behaviour with large lateral length scale patterns reappearing (Fig. 1d). At these high concentrations, the patterns consist of thicker multilayer structures in contrast to the monolayer patterns observed at lower concentrations.

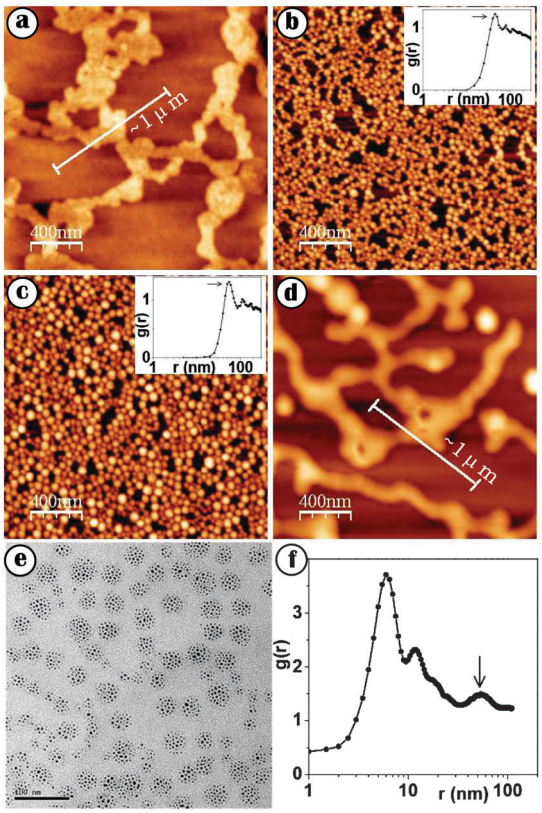

Fig. 1 (a)–(d) AFM images of films prepared from PGNP3K solutions of different spreading concentrations, (a) 0.05 mg ml^{-1}; (b) 0.5 mg ml^{-1}; (c) 0.75 mg ml^{-1}; (d) 1.6 mg ml^{-1}. The white lines in (a) and (d) indicate the large length scale of patterns. Pair correlation functions $g(r)$ of clusters are shown in the insets of (b) and (c). (e) TEM image of the PGNP3K film prepared from 0.5 mg ml^{-1} solution. (f) $g(r)$ of individual PGNPs plotted in the linear-log scale where the arrow indicates the peak corresponding to the distribution of clusters.

To study the distribution of the individual PGNPs and their clusters, we prepare the films on TEM grids. The TEM image of PGNP3K film is shown in Fig. 1e and the corresponding pair correlation function, $g(r)$, of PGNPs is given in Fig. 1f. The self-assembly of the PGNPs is clearly visible from their regular arrangement within individual clusters that in turn are organized on a larger length scale implying hierarchical structuring. The pronounced maximum in $g(r)$ at 6 nm, corresponds to the particle spacing within the individual clusters, while the less pronounced peak at a larger distance of 50 nm (marked by an arrow pointing downwards) indicates the spacing between the clusters. The interparticle distance is close to the expected value of the melt diameter of the PGNPs as extracted from small angle X-ray scattering (SAXS).

‡ M_w: molecular weight of the grafted polymer chains, d_c: diameter of the gold nanocore, σ: number of polymer chains per unit area of the core, d_{melt}: diameter of PGNPs in the melt state and R_h: hydrodynamic radius.

However, the actual value of the PGNP diameter could be underestimated since both TEM and SAXS measure the core–core separation and in case of chain interpenetration the diameter will turn out to be less than the actual value. Since the gold content in the prepared PGNPs is ~0.24% which is below the required 0.5 vol% for hexagonal ordering,[14,15] we believe that the mechanism of pattern formation observed in our experiments is due to the intrinsic nature of grafted PST chains. To verify this, we prepared a set of films from bare PST of the same M_w as the grafted chains (PS3K), following the same procedure. Interestingly, qualitatively similar features were observed in the morphology of the transferred films for both bare PST and PGNPs. Fig. 2 clearly shows the switch over from larger length scale patterns at low concentrations to smaller length scales and also the re-entrant behaviour for higher concentrations. Similar morphological transitions are also observed for the PGNP53K suspension as well (see Section 3 of the ESI†).

The independence of pattern formation of transfer surface pressure (see the ESI,† Section 4) implies that without the solvent chloroform there are no significant forces that can lead to self-assembly. It thus becomes clear that the observed pattern formation is driven by instabilities within the chloroform suspension on water, as it evaporates. Modeling of the entire hydrodynamic process of a highly volatile thin film suspension is fairly complex and has not been successfully attempted to the best of our knowledge. However, the time and length scales for the onset of instabilities in thin non-volatile single component films have been well studied.[16–20] It is well known that the growth rate of the fastest growing mode of instability in unstable thin liquid films is $\beta \sim h^{-5}$, where h is the film thickness.[20] However, for a highly volatile solvent like chloroform β will be largely dominated by the evaporation rate and hence dewetting is unlikely to set in unless the film thins below a certain thickness. This of course will only lead to a single instability length scale corresponding to dewetting and is usually found to be in the range of a few μm.[18,20] Neither the concentration-dependent crossover to a much smaller length scale nor the re-entrant behaviour observed in our experiments can emerge from such a model. An additional length scale can only emerge if there are additional instability mechanisms apart from dewetting. In our case, this mechanism is the bulk decomposition of the polymer (or PGNP) suspension. Polystyrene in chloroform is under good solvent conditions and is unlikely to lead to any instabilities in the bulk. Again, evaporation plays a critical role since when the film thickness becomes comparable to either the chain dimension or the average interparticle (interchain) spacing then the polymer segments become exposed to either water or air both of which are poor solvents for PS. Thus, bulk decomposition mediated instabilities are also expected to be effective only below a certain thickness of the suspension film. Hence, to understand the physics of the lateral pattern formation, essentially length scale switch-over and the re-entrant behaviour, observed in experiments, we make the following simplifying assumptions: (i) evaporation essentially facilitates only the reduction of the initial suspension film thickness and can be decoupled from dewetting or bulk-decomposition for thinner films and (ii) since the experimental pattern transitions are engendered through composition variation, the suspension behaviour can be captured at fixed film thickness although in experiments the onset thickness for instabilities to set in could vary slightly with concentration. We argue that this is justifiable since the bulk compositional instabilities are likely to take place only in the thickness regime of 20–50 nm which we believe dictates the onset of the confinement regime since average interparticle spacing is estimated to be in this range (at the experimental suspension concentrations).

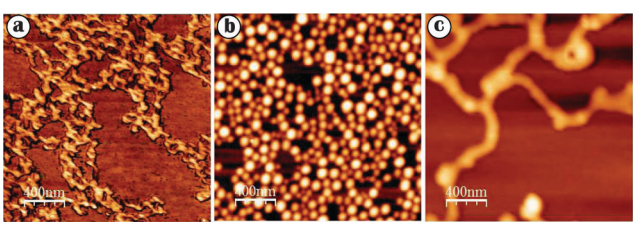

Fig. 2 AFM images of PS3K thin films for spreading concentrations, (a) 0.05 mg ml^{-1}, (b) 0.5 mg ml^{-1} and (c) 3 mg ml^{-1}.

Thus, we employ here a thin film hydrodynamic model to take into account only the dewetting and compositional instabilities. We use this simplified linear model to capture an otherwise complex non-linear hydrodynamic process with the sole intention of providing a physically intuitive minimal framework which captures the major experimental observations: (a) onset of a nanoscale pattern from a microscale dewetting pattern and (b) emergence of re-entrant behaviour.

3.2 Theoretical analysis

We investigate the dewetting and compositional instability of thin films as described by the gradient dynamics model for the coupled evolution of the film thickness h and local vertically averaged polymer concentration (volume fraction) ϕ.[21–24] In particular, using the theoretical model described below, we demonstrate the physical phenomenon, of transition in wavelength observed in experiments, using a film thickness of 30 nm. We model the thin film of polymer solution/nanoparticle suspension on water by considering the liquid substrate to be immobile and the solution as a binary mixture consisting of polystyrene (PS) and chloroform. The polymer–polymer and polymer–chloroform interactions are taken into account in the total free energy of the film.

For our binary mixture film, the governing free energy functional can be written as,[22]

$$F[h,\phi] = \int \left[\frac{\gamma}{2}|\nabla h|^2 + f(h,\phi) + h f_B(\phi,\nabla\phi)\right] \mathrm{d}A, \qquad (1)$$

where the first term accounts for the local surface energy where γ is the solution–air interface tension, $f(h, \phi)$ is the wetting energy of the film on water and $f_B(\phi, \nabla\phi)$ is the bulk film energy. For the wetting energy in the partially wetting case, we assume the simple form due to van der Waals forces[25] with the effective Hamaker constant of the polymer solution, $A(\phi)$, calculated from the Lifshitz theory within the effective medium approximation.[26]

For a thin film of the PS–chloroform mixture on a water substrate, $A(\phi) = A_0(1 + M_1\phi)$ where $A_0 = 1.08 \times 10^{-20}$ Nm and $M_1 = 1.34$ (see the ESI†). As the considered mean film thicknesses are well above 10 nm, we neglect the polar interactions due to the aqueous substrate which play a significant role only at smaller h.[27] The bulk free energy of the polymer solution consists of the Flory–Huggins energy and the energetic cost resulting from polymer concentration gradients,[28,29]

$$f_B(\phi, \nabla\phi) = \frac{k_B T}{a^3}\Big(g_{FH}(\phi) + \kappa(\phi)|\nabla\phi|^2\Big), \quad (2)$$

$$g_{FH}(\phi) = \frac{\phi}{N}\ln(\phi) + (1-\phi)\ln(1-\phi) + \chi\phi(1-\phi). \quad (3)$$

The Flory–Huggins energy, $g_{FH}(\phi)$, incorporates the conformational entropy of polymer chains (first term in eqn (3)), the translational entropy of solvent molecules (second term) and the interaction energy between the polymer and the solvent (last term). Here, N is the degree of polymerization and χ is the Flory interaction parameter. The latter is small for polymers dissolved in a good solvent, reaches 0.5 for an ideal solvent and increases further for poor solvents.[28] For PS in chloroform $\chi = 0.4$ and for PS in water it is $\chi = 4$.[30] For our experimental system, we therefore expect that the evaporating un-grafted polystyrene (and similarly PGNP) suspension in chloroform on water has due to confinement effects an effective Flory interaction parameter, χ_{film}, that drifts from 0.4 to 4, the latter value corresponding to the PGNPs at the air–water interface after the complete evaporation of chloroform. Similar variations in the effective interaction have been suggested previously for evaporating solution films.[8,31] Unlike for a colloidal solution, the coefficient of the concentration gradient term in the free energy, κ, is a function of concentration, the Flory parameter and the range of energetic interactions between monomers (r_0),[32] $\kappa(\phi) = \frac{\chi {r_0}^2}{6} + \frac{a^2}{36\phi(1-\phi)}$. This is due to the constraint on monomers in a polymer chain because of their connectivity. The coupled evolution equations for height h and effective polymer layer thickness ($\psi = h\phi$) are,[21]

$$\frac{\partial h}{\partial t} = \nabla\cdot\left(Q_{hh}\nabla\frac{\delta F}{\delta h} + Q_{h\psi}\nabla\frac{\delta F}{\delta \psi}\right), \quad (4)$$

$$\frac{\partial \psi}{\partial t} = \nabla\cdot\left(Q_{\psi h}\nabla\frac{\delta F}{\delta h} + Q_{\psi\psi}\nabla\frac{\delta F}{\delta \psi}\right), \quad (5)$$

where Q is the mobility matrix, which is given by,

$$Q = \begin{pmatrix} Q_{hh} & Q_{h\psi} \\ Q_{\psi h} & Q_{\psi\psi} \end{pmatrix} = \frac{1}{3\eta}\begin{pmatrix} h^3 & h^2\psi \\ h^2\psi & h\psi^2 + \frac{a^3\psi}{2\pi R_h} \end{pmatrix}. \quad (6)$$

Here, a is the monomer length and R_h is the hydrodynamic radius of polymer chains. We note here that, for a given system, Q essentially modifies only the timescales but does not affect instability thresholds and the corresponding critical length scale of the instabilities. We expect a small influence of the substrate characteristics (solid *vs.* liquid) on the fastest growing wavelength.

We perform LSA of the evolution equations (eqn (4) and (5)) to obtain the dispersion curves, *i.e.* the dependence of the largest growth rate of fluctuations on their wave number, k. The corresponding wavelength, λ, indicates the length scale that is most likely to emerge in the pattern formation. We note here that, although the nonlinear growth of instabilities may possibly involve vertical packing and local organization of the solute that is not accounted for in the present mean field continuum model, the system is arrested in the energy minimum corresponding to the LSA wavelengths and therefore would result in little variations in the final pattern lengthscales.

First, we analyze the influence of χ in the earlier deduced physically plausible range $\in$ (0.4, 4). Fig. 3 shows dispersion curves for un-grafted polystyrene solution (PS3K) at fixed polymer concentration $\phi = 0.1$ and film thickness $h = 30$ nm with the varying Flory interaction parameter. Other model parameters for PS solution are discussed in Section 5 of the ESI.† At low values of χ($\chi < 0.7292$), we obtain dispersion curves with a single maximum that corresponds to the large length scale, λ_h, related to dewetting. Here, $\lambda_h \approx 7$ μm, *i.e.* of the order of the experimentally observed length scale ~1 μm at low and high concentrations (see Fig. 1 and 2). At the critical value $\chi_c = 0.7292$, the dispersion curve becomes bimodal, *i.e.*, a second maximum emerges at a smaller length scale ($\lambda_\phi \sim 60$ nm $\ll \lambda_h$). This switch over of the length scale from large to small captures the experimental observations shown in Fig. 1a and b for PGNPs and Fig. 2a and b for un-grafted PS. Also, the order of change in the length scale is in agreement with the experimental observations, *i.e.* from ~μm to around 50 nm. This occurs when the effective solvent–solute interaction overcomes the entropic Brownian motion. For increasing χ, the scale λ_ϕ slowly decreases while the corresponding growth rate increases and the composition mode becomes dominant.

LSA results for a range of ϕ values are given in Fig. 4 and agree, as explained next, with the experimental observations. Note, that bimodal dispersion curves are not observed for binary mixtures if their bulk free energy is purely entropic and hence no bulk decomposition can occur.[22] However, for our experimental systems, the interaction energy plays an important role since the solvent quality is changing drastically as the film thickness decreases due to evaporation. In the bulk free energy, there is a competition between entropy (Brownian forces) and enthalpy (effective solvent–solute interaction). When the Flory interaction parameter is large enough, the thin

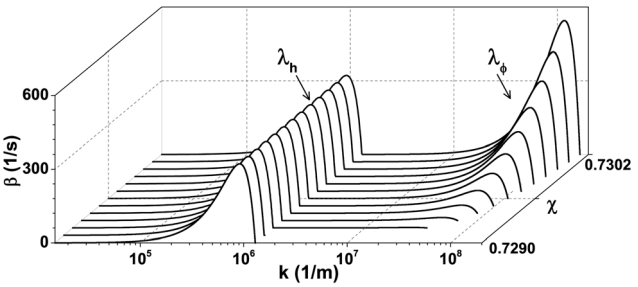

Fig. 3 Dispersion curves of the PS3K thin film for h = 30 nm and ϕ = 0.1 for χ ranging from 0.729 to 0.7302.

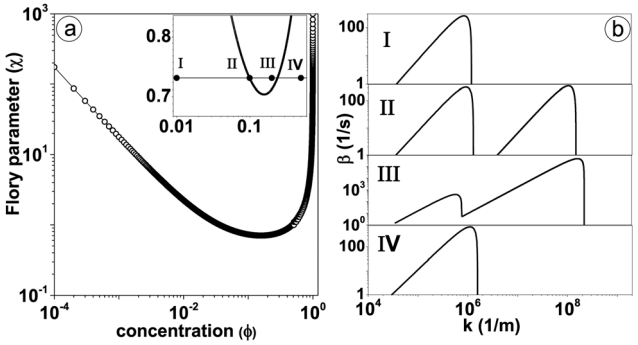

Fig. 4 (a) Compositional stability diagram of PS3K in the space spanned by ϕ and χ. The inset gives a zoom of the stability onto the values of ϕ for which dispersion relations are calculated. (b) Dispersion curves of PS3K for 4 different concentrations 0.01 (I), 0.1 (II), 0.2 (III), 0.5 (IV) at χ = 0.73 and h = 30 nm as the log–log plot, showing the transitions in the dominating instabilities.

film solution becomes unstable and the phases separate. So the appearance of a smaller length scale can be ascribed to the decomposition of the polymer solution that is unstable when $\partial_{\phi\phi} g_{\mathrm{FH}} \leq 0$ and stable otherwise. Based on the above argument, Fig. 4a gives the phase diagram for the polymer solution indicating the boundary of the compositional stability of a polymer solution. For each polymer concentration ϕ, there is a critical value of the Flory interaction parameter χ_c above which the dispersion curve becomes bimodal. The competition between polymer entropy, solvent entropy and interaction energy determines how χ_c varies with ϕ. As chloroform evaporates, the concentration of the PST increases and due to stronger confinement the effective χ increases and the system crosses the phase boundary in Fig. 4a. Note that the exact value of χ for a particular h and ϕ is not known, however, the variation in length scales with concentration can be studied. Interestingly, the above phase diagram also suggests the possibility of the suppression of the phase separation as indicated by the right arm of the phase boundary in Fig. 4a. To investigate this further, we perform LSA for a range of concentrations such that both the initial switch over from the large to small lengthscale, as well as the re-entrant behaviour suggested by the phase-diagram are captured. As an example, Fig. 4b shows how the small length scale appears and again disappears when increasing the concentration over a range similar to the experimental one (stated above for h = 30 nm and χ = 0.73, also *cf.* labels I to IV in the inset of Fig. 4a). For increasing concentrations at the constant χ the dispersion curves first exhibit a transformation from unimodal to bimodal, due to the onset of the compositional instability (see Fig. 4b). Then, at higher concentrations, a re-entrant unimodal dewetting instability occurs due to the reduced effective solvent–solute interaction. The variation in the ratio of the growth rates at λ_h and λ_ϕ is given in the ESI.† It should be noted here, as has been alluded to earlier, the model uses an effective representation of the actual experimental system in terms of the assumption of constants h and χ for a range of concentrations. In actual experiments χ is likely to be a function of h and the h at which the suspension film becomes unstable might depend on ϕ. However, within the range of experimental value of ϕ used the interparticle spacing changes by a very small amount and it is unlikely that the onset of film thickness and hence χ will vary significantly with ϕ in the experimental parameter range. As similar calculations for a different film thickness (h = 50 nm) and χ show (see the ESI†), the overall nature of the ϕ dependent phase diagram is unaltered by the use of these slightly different h and χ values – only the ratio of growth rates β_ϕ and β_h changes. Thus the simplified LSA model seem to be fairly successful in capturing the essential physics behind the two major experimental observations – (a) dramatic concentration dependent pattern formation length scale transition and (b) reemergence of a single large length scale for higher concentration.

In this study, we have presented experimental observations of interesting evaporation-mediated formation of hierarchical patterns in binary mixtures. For low concentrations a large dewetting length scale is observed and with an increase in concentration a switch over to patterns with smaller length scales occurs. At even higher concentrations, an interesting re-entrant behaviour in the pattern length scale is observed and patterns with larger dewetting length scales $\sim$μm are obtained.

We employed a thin film model to understand the underlying mechanisms of pattern formation in binary mixture films observed in our experiments. Linear stability analysis of our mesoscopic model well captures the occurring pattern length scales, in particular, the possibility of two disparate length scales separated by one to two orders of magnitude whose occurrence depends on the concentration of the polymer in the confined solution. It also captures the re-entrant behaviour at larger concentrations.

Although LSA predicts the conditions at which dewetting and decomposition instabilities become equally likely what results in bimodality, the exact experimental realization of such conditions is difficult. For instance, with increasing χ the growth rate of the small length scale increases resulting in a weaker modulation of the small scale structure on the large length scale. Nevertheless, one sees clear evidence for the bimodal nature of the structures, *e.g.*, in large area scan images (see the ESI†). For very high concentrations, χ_c is large such that $\chi_{\mathrm{film}} < \chi_c$ during the entire evolution leading to the formation of pure dewetting patterns. In this way, the experimentally observed re-entrance can be clearly described. We emphasize that the phase separation is not merely due to high concentration but essentially due to confinement effects resulting from progressively thinning films sandwiched between bad solvents.

4 Conclusion

We have shown that a film of a suspension of polymer grafted gold nanoparticles at the air–water interface can be utilized to create two-dimensional nanostructures with a remarkable variation in the pattern length scales, including bimodal patterns and re-entrant behaviour. We explain the observed hierarchical patterns in terms of a gradient dynamics model consisting of coupled evolution equations for the height of the suspension film and the concentration of polymers. We believe that the discussed

competition between dewetting and decomposition instabilities is quite generic and will occur in many situations where films of solutions undergo a decrease in solvent quality due to confinement effects.

Acknowledgements

The authors acknowledge the Advanced Facility for Microscopy and Microanalysis (AFMM) and the Center for Excellence in Nanoscience and Engineering (CeNSE), IISc for providing access to TEM and DLS facilities, respectively, and thank Dr M. Haridas for expert assistance with TEM measurements.

References

1 P. Ball and N. R. Borley, *The self-made tapestry: pattern formation in nature*, Oxford University Press Oxford, 1999, vol. 198.
2 G. M. Whitesides and B. Grzybowski, *Science*, 2002, **295**, 2418–2421.
3 K. J. Bishop, C. E. Wilmer, S. Soh and B. A. Grzybowski, *Small*, 2009, **5**, 1600–1630.
4 M. Grzelczak, J. Vermant, E. M. Furst and L. M. Liz-Marzán, *ACS Nano*, 2010, **4**, 3591–3605.
5 W. M. Gelbart, R. P. Sear, J. R. Heath and S. Chaney, *Faraday Discuss.*, 1999, **112**, 299–307.
6 D. V. Talapin, J.-S. Lee, M. V. Kovalenko and E. V. Shevchenko, *Chem. Rev.*, 2009, **110**, 389–458.
7 J. A. Fan, C. Wu, K. Bao, J. Bao, R. Bardhan, N. J. Halas, V. N. Manoharan, P. Nordlander, G. Shvets and F. Capasso, *Science*, 2010, **328**, 1135–1138.
8 E. Rabani, D. R. Reichman, P. L. Geissler and L. E. Brus, *Nature*, 2003, **426**, 271–274.
9 A. Dong, J. Chen, S. J. Oh, W.-K. Koh, F. Xiu, X. Ye, D.-K. Ko, K. L. Wang, C. R. Kagan and C. B. Murray, *Nano Lett.*, 2011, **11**, 841–846.
10 S. Kinge, M. Crego-Calama and D. N. Reinhoudt, *ChemPhysChem*, 2008, **9**, 20–42.
11 C. P. Martin, M. O. Blunt, E. Pauliac-Vaujour, A. Stannard, P. Moriarty, I. Vancea and U. Thiele, *Phys. Rev. Lett.*, 2007, **99**, 116103.
12 J. Huang, F. Kim, A. R. Tao, S. Connor and P. Yang, *Nat. Mater.*, 2005, **4**, 896–900.
13 A. Stannard, *J. Phys.: Condens. Matter*, 2011, **23**, 083001.
14 H. Yockell-Lelièvre, J. Desbiens and A. M. Ritcey, *Langmuir*, 2007, **23**, 2843–2850.
15 G. Muralidharan, N. Bhat and V. Santhanam, *Nanoscale*, 2011, **3**, 4575–4579.
16 A. Vrij, *Discuss. Faraday Soc.*, 1966, **42**, 23–33.
17 E. Ruckenstein and R. K. Jain, *J. Chem. Soc., Faraday Trans. 2*, 1974, **70**, 132–147.
18 A. Oron, S. H. Davis and S. G. Bankoff, *Rev. Mod. Phys.*, 1997, **69**, 931.
19 R. Craster and O. Matar, *Rev. Mod. Phys.*, 2009, **81**, 1131.
20 A. Sharma and R. Khanna, *Phys. Rev. Lett.*, 1998, **81**, 3463.
21 U. Thiele, *Eur. Biophys. J.*, 2011, **197**, 213–220.
22 U. Thiele, D. V. Todorova and H. Lopez, *Phys. Rev. Lett.*, 2013, **111**, 117801.
23 N. Clarke, *Macromolecules*, 2005, **38**, 6775–6778.
24 L. Ó. Náraigh and J.-L. Thiffeault, *Nonlinearity Biol., Toxicol., Med.*, 2010, **23**, 1559.
25 J. N. Israelachvili, *Intermolecular and surface forces: revised third edition*, Academic press, 2011.
26 D. V. Todorova, PhD thesis, Loughborough University, United Kingdom, 2013.
27 A. Sharma, *Langmuir*, 1993, **9**, 861–869.
28 P.-G. De Gennes, *Scaling concepts in polymer physics*, Cornell University Press, 1979.
29 S. Safran, *Statistical Thermodynamics of Surfaces and interfaces*, Addison-Wesley, New York, 1994, vol. 103.
30 J. Brandrup, E. H. Immergut, E. A. Grulke, A. Abe and D. R. Bloch, *Polymer handbook*, Wiley New York, 1999, vol. 89.
31 G. Ge and L. Brus, *J. Phys. Chem. B*, 2000, **104**, 9573–9575.
32 R. A. Jones and R. W. Richards, *Polymers at surfaces and interfaces*, Cambridge University Press, 1999.

